J Neuropathol Exp Neurol
Vol. 79, No. 2, February 2020, pp. 163–175
doi: 10.1093/jnen/nlz123

ORIGINAL ARTICLE

From the Entorhinal Region via the Prosubiculum to the Dentate Fascia: Alzheimer Disease-Related Neurofibrillary Changes in the Temporal Allocortex

Heiko Braak, MD and Kelly Del Tredici, MD, PhD

Abstract

The pathological process underlying Alzheimer disease (AD) unfolds predominantly in the cerebral cortex with the gradual appearance and regional progression of abnormal tau. Intraneuronal tau pathology progresses from the temporal transentorhinal and entorhinal regions into neocortical fields/areas of the temporal allocortex. Here, based on 95 cases staged for AD-related neurofibrillary changes, we propose an ordered progression of abnormal tau in the temporal allocortex. Initially, abnormal tau was limited to distal dendritic segments followed by tau in cell bodies of projection neurons of the transentorhinal/entorhinal layer pre-α. Next, abnormal distal dendrites accumulated in the prosubiculum and extended into the CA1 stratum oriens and lacunosum. Subsequently, altered dendrites developed in the CA2/CA3 stratum oriens and stratum lacunosum-moleculare, combined with tau-positive thorny excrescences of CA3/CA4 mossy cells. Finally, granule cells of the dentate fascia became involved. Such a progression might recapitulate a sequence of transsynaptic spreading of abnormal tau from 1 projection neuron to the next: From pre-α cells to distal dendrites in the prosubiculum and CA1; then, from CA1 or prosubicular pyramids to CA2 principal cells and CA3/CA4 mossy cells; finally, from CA4 mossy cells to dentate granule cells. The lesions are additive: Those from the previous steps persist.

Key Words: Alzheimer disease, Ammon's horn, Dendritic tau, Neurofibrillary, Neuropil threads, Pretangles, Thorny excrescences.

INTRODUCTION

Sporadic Alzheimer disease (sAD) is a human tauopathy that selectively involves specific neuronal types while sparing others (1–4). Generally speaking, familial cases, which include early- and late-onset types, account for <3% of all AD cases (5–7), whereas the remainder are sporadic (idiopathic) without manifest heritability. Particularly, susceptible are late-developing and late-maturing projection neurons that generate—in relation to the size of their cell body—a long and sparsely myelinated axon (3, 8). With minor exceptions, local circuit neurons are resistant (3). The predictable pattern of the tau lesions makes it possible to track the progression and to distinguish different neuropathological stages (9–12). The lesions include AT8-immunopositive nonargyrophilic pretangles (13–15) that convert into argyrophilic filamentous accumulations of abnormal tau in dendrites (neuropil threads [NTs]) (16, 17), and cell somata (neurofibrillary tangles [NFTs]) (9, 18). Abnormal tau in axons generally resists conversion into argyrophilic tau except in terminal axons of neuritic plaques (3). The present study presents a sequence of neuronal involvement within the temporal allocortex with a focus on the earliest changes, namely, the development of abnormal tau in distal segments of dendrites (15, 19).

Unidirectional connectivities are known to exist in the temporal allocortex that begin in the dentate fascia (df) and project via mossy fibers, Schaffer collaterals, and the ammonic-subicular pathway to the subiculum ([20]; see also Supplementary Data). Here, we propose a progression of tau lesions that proceeds in the opposite direction, namely, from the entorhinal cortex to the prosubiculum and CA1, and, from there, to CA2-CA4 and then the df. This sequence suggests the existence of connectivities within the temporal allocortex that are still partially uncertain (Fig. 1).

MATERIALS AND METHODS

Study Cohort

This retrospective study was conducted in compliance with university ethics committee guidelines as well as with German federal and state law governing human tissue usage. Informed written permission for autopsy was obtained from all patients and/or their next of kin. The cohort included 95 individuals (52 females, 43 males, age range 34–97 ± 13.1 years of age; mean age 74.5 years). The postmortem interval to autopsy ranged from 5 to 107 hours, with a median of 41 hours for all cases. All brains were staged for tau pathology corresponding to NFT stages I–VI (Roman numerals) and Aβ phases 0–5 (Arabic numerals) (9, 12, 21). Individuals with neuropathologically confirmed preclinical or clinical

From the Department of Neurology, Clinical Neuroanatomy, Center for Biomedical Research, University of Ulm, Ulm, Germany (HR, KDT).
Send correspondence to: Heiko Braak, MD, Clinical Neuroanatomy, Center for Biomedical Research, Helmholtzstrasse 8/1, 89081 Ulm, Germany; E-mail: heiko.braak@uni-ulm.de
This study was supported, in part, by the Hans & Ilse Breuer Foundation (Frankfurt am Main).
The authors have no duality or conflicts of interest to declare.
Supplementary Data can be found at academic.oup.com/jnen.

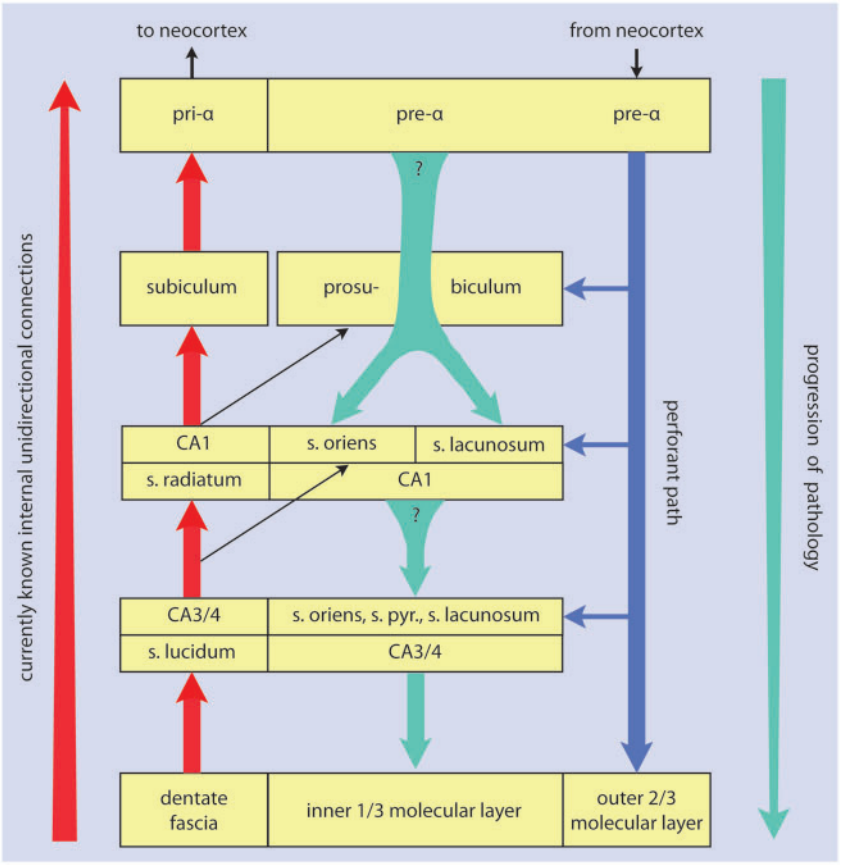

FIGURE 1. Summary diagram of temporal lobe allocortical connectivities. The direction of the main efferent projections is indicated by the red arrow at the far left. Granule cells of the dentate fascia project via mossy fibers to CA3 and CA4 projection neurons. Axons of these cells contribute to the alveus and give off Schaffer collaterals to CA1 pyramidal cells. These, in turn, project via the ammonic-subicular pathway to the prosubiculum/subiculum, and subicular efferents reach the deep layer pri-α of the entorhinal region (short red arrows). Outer layers of the entorhinal and transentorhinal regions project via the perforant path (blue arrow) to the Ammon's horn and predominantly to the dentate fascia. The progression of the sAD-associated pathology is indicated by the green arrow at the far right. Shorter green arrows between the boxes indicate the here hypothesized projections from pre-α cells to the prosubiculum and both the stratum oriens and stratum lacunosum of CA1, as well as the hypothetical projections from prosubicular and/or CA1 pyramidal cells to the stratum oriens, stratum lacunosum, and to thorny excrescences of CA3/CA4 projection neurons. Question marks indicate uncertainties regarding the existence of these connections. A known pathway is given off from CA3/CA4 mossy cells to the inner one-third of the dentate molecular layer.

synucleinopathies or frontotemporal lobar dementia-TDP were excluded from the study. Other exclusionary criteria were the presence of tauopathies other than sAD, for example, argyrophilic grain disease (22), Niemann-Pick disease type C (23), subacute sclerosing panencephalitis, progressive supranuclear palsy, Pick disease, or corticobasal degeneration (24). A summary of the demographic and neuropathological data, including NFT and Aβ stages, apolipoprotein E status, and the presence of hippocampal sclerosis, is provided for all cases in the Table. Hippocampal (or Ammon's horn) sclerosis, which is marked by severe neuronal loss and gliosis in sector CA1 and/or the subiculum, is considered a neurodegenerative substrate of cognitive decline (25–27).

Genetic Analysis

Apolipoprotein E status was available for all individuals studied (Table). The ε4 allele is a major genetic risk factor for sAD (28–30) and for TDP-43 proteinopathy (31). An *APOE* genotyping was performed using a seminested polymerase chain reaction assay and restriction isotyping with restriction enzyme *HhaI*, as elsewhere (32). Genomic DNA was extracted from formaldehyde-fixed and paraffin-embedded brain or liver specimens.

Tissue Fixation, Embedding, and Sectioning

The brains were fixed by immersion in a 4% aqueous solution of formaldehyde for 14 days prior to dissection. The following tissue blocks required for neuropathological diagnosis and staging were dissected: 2 transversally cut blocks through the temporal lobe, the first through the uncal portion of the hippocampus, including the adjoining parahippocampal and occipito-temporal gyri, the second through the hippocampus at the latitude of the lateral geniculate body. A third block was cut from basal portions of the occipital lobe. The cut was

TABLE. Demographic and Neuropathological Data From the 95 Cases Studied

Case	Gender	Age	NFT Stage	Aβ Phase	APOE	AGD	TDP-43	HS
1	Female	34	I	0	3/4	0	0	0
2	Female	55	I	0	3/3	0	0	0
3	Male	58	I	1	3/4	0	0	0
4	Male	60	I	1	3/3	0	0	0
5	Male	61	I	0	3/3	0	0	0
6	Female	65	I	0	3/4	0	0	0
7	Male	69	I	0	3/3	0	0	0
8	Male	82	I	0	3/4	0	0	0
9	Male	37	II	0	3/3	0	0	0
10	Female	48	II	0	3/3	0	0	0
11	Male	53	II	0	3/4	0	0	+
12	Female	56	II	0	3/4	0	0	0
13	Male	56	II	0	3/3	0	0	0
14	Male	56	II	0	3/3	0	0	0
15	Male	61	II	0	3/3	0	0	0
16	Male	61	II	0	3/3	0	0	0
17	Male	62	II	0	3/3	0	0	0
18	Female	62	II	0	3/3	0	0	0
19	Male	62	II	0	3/3	0	0	0
20	Male	62	II	2	3/4	0	0	0
21	Female	63	II	0	2/3	0	0	0
22	Male	64	II	0	3/3	0	0	0
23	Male	64	II	0	3/3	0	0	+
24	Male	64	II	1	3/4	0	0	0
25	Male	65	II	0	3/3	0	0	0
26	Female	82	II	1	3/3	0	0	0
27	Male	85	II	0	2/3	0	0	0
28	Female	86	II	2	3/3	0	0	0
29	Female	87	II	0	3/3	0	0	0
30	Male	87	II	2	3/4	0	0	0
31	Male	52	III	0	3/3	0	0	0
32	Male	55	III	1	3/4	0	0	0
33	Female	58	III	0	3/3	0	+	0
34	Male	66	III	0	2/3	0	0	+++
35	Female	67	III	0	3/4	0	0	0
36	Female	68	III	3	3/4	0	0	0
37	Female	68	III	1	3/4	0	0	0
38	Female	68	III	2	3/4	0	0	0
39	Male	69	III	0	2/3	0	0	+
40	Female	69	III	5	4/4	0	0	0
41	Female	70	III	0	3/3	0	0	0
42	Male	71	III	0	3/3	0	0	+
43	Male	71	III	3	4/4	0	0	0
44	Female	76	III	1	3/3	0	0	0
45	Female	83	III	0	3/4	0	0	0
46	Female	86	III	3	3/4	0	0	0
47	Female	87	III	0	3/4	0	0	0
48	Female	88	III	0	2/3	0	0	0
49	Female	88	III	0	3/3	0	0	+
50	Male	89	III	0	3/3	0	0	0
51	Female	89	III	0	3/3	0	+++	+++
52	Male	91	III	0	3/3	0	0	+
53	Male	93	III	0	3/3	0	0	0
54	Male	71	IV	3	3/3	0	0	0

(continued)

TABLE. Continued

Case	Gender	Age	NFT Stage	Aβ Phase	APOE	AGD	TDP-43	HS
55	Male	72	IV	2	3/3	0	0	0
56	Female	75	IV	5	4/4	0	0	0
57	Female	78	IV	3	3/4	0	0	0
58	Male	83	IV	3	3/3	0	0	0
59	Female	84	IV	2	3/4	0	0	0
60	Female	84	IV	2	4/4	0	0	++
61	Female	86	IV	3	3/3	0	0	0
62	Female	86	IV	3	3/4	0	+++	+
63	Female	89	IV	3	3/3	0	0	0
64	Male	90	IV	3	3/4	0	0	0
65	Female	55	V	5	3/3	0	0	0
66	Male	58	V	2	3/4	0	0	0
67	Female	72	V	4	3/3	0	0	0
68	Female	73	V	5	3/3	0	0	0
69	Female	75	V	2	4/4	0	0	0
70	Female	76	V	4	3/4	0	0	0
71	Female	78	V	4	3/3	0	+++	+
72	Female	78	V	0	3/3	0	0	++
73	Female	78	V	3	3/3	0	0	0
74	Male	78	V	5	3/4	0	0	+
75	Male	80	V	2	3/3	0	0	0
76	Female	81	V	4	3/3	0	0	0
77	Female	82	V	3	3/3	0	+	0
78	Male	82	V	4	3/3	0	0	0
79	Male	84	V	3	3/4	0	++	0
80	Female	85	V	3	3/4	0	0	+
81	Female	87	V	4	2/4	0	+++	0
82	Female	88	V	3	3/3	0	0	0
83	Female	88	V	5	3/3	0	0	0
84	Male	88	V	3	2/2	0	0	0
85	Male	88	V	4	2/3	0	0	0
86	Male	89	V	3	3/3	0	0	0
87	Female	89	V	4	3/3	0	++	0
88	Female	90	V	2	3/3	0	0	0
89	Female	92	V	4	3/3	0	0	0
90	Male	93	V	2	3/4	0	0	+++
91	Female	96	V	5	3/3	0	0	0
92	Female	97	V	3	3/3	0	0	0
93	Male	75	VI	4	3/3	0	0	0
94	Female	83	VI	3	3/4	0	+++	+
95	Female	85	VI	4	3/4	0	++	+

The cohort consisted of 52 females and 43 males (age range 34–97 ± 13.1 years of age; mean age 74.5 years).

Its composition reflects the fact that early neurofibrillary changes corresponding to NFT stages I–II are already present in the third and fourth decades of life. NFT stages and Aβ phases increase with age. The disease process underlying sporadic AD develops over a period of decades (11).

NFT, neurofibrillary tangle stages I–VI; Aβ, amyloid-β deposition phases 0–5; AGD, argyrophilic grain disease; HS, hippocampal sclerosis.

oriented perpendicular to the calcarine fissure and included the neocortex covering the lower bank of the calcarine fissure together with the adjoining basal occipital gyri. It contained portions of the peristriate region, the parastriate, and striate areas (9, 10).

The 3 blocks were embedded in polyethylene glycol (PEG 1000, Merck, Carl Roth Ltd, Karlsruhe, Germany) (33), and sectioning was performed with a tetrander (Jung, Heidelberg, Germany) at a thickness of 100 µm, as described previously (34). Additional unstained 100-µm tissue sections were stored for subsequent use in a 4% aqueous solution of formaldehyde at 8–20°C. The unconventional section thickness was chosen because it allows for the optical superimposition of large numbers of biological structures, including pathological ones and nerve cells with their entire dendritic arbor and substantial portions of the arborizations around each neuron (3, 34).

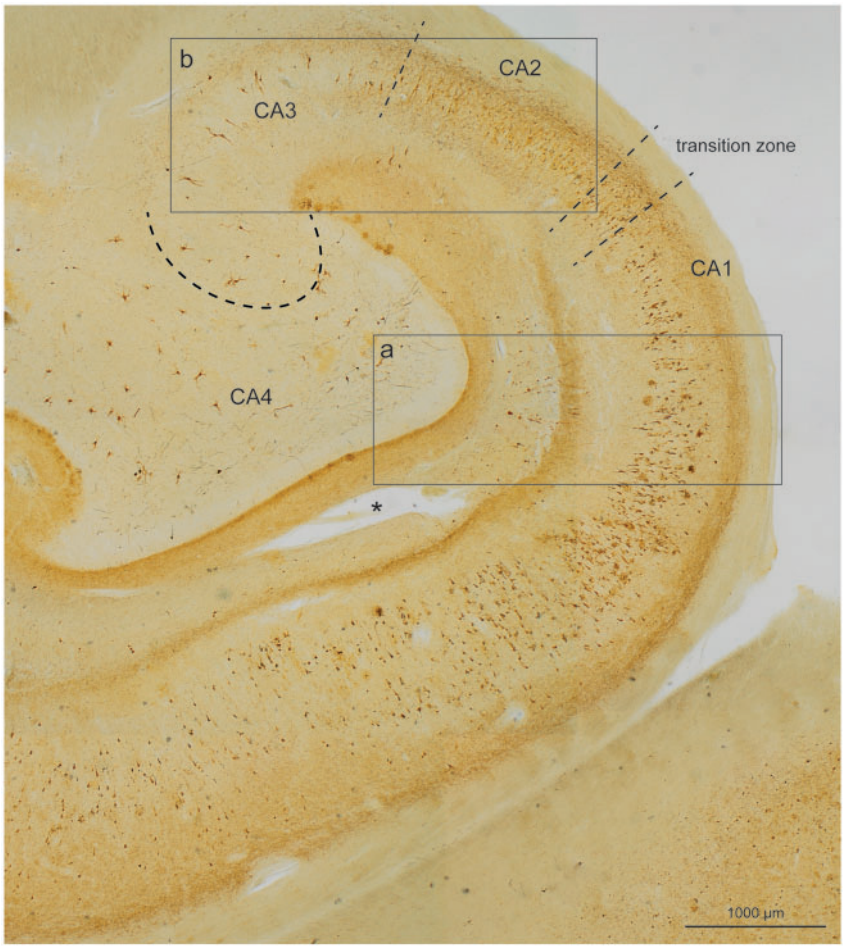

FIGURE 2. Overview of large portions of the Ammon's horn and dentate fascia in a section of 100-µm thickness using an immunoreaction for abnormally phosphorylated tau protein (AT8) (case 45, female, age 83, NFT III, Aβ 0). Broken lines mark a transition zone between CA1 and CA2. Additional broken lines indicate the border between CA2 and CA3 and between CA3 and CA4. The image shows the presence of very numerous distal dendritic segments (neuropil threads [NTs]) that form 2 stripe-like zones above and below the pyramidal layers, and which develop during the Alzheimer disease-related pathological process. A deep stripe runs within the stratum oriens of CA1, CA2, and CA3, whereas a superficial and slightly less dense stripe runs through the stratum lacunosum of CA1, continuing more faintly into CA2 and CA3. Framed areas are shown in greater detail in Figure 3a and b.

Staining and Immunocytochemistry

One set of free-floating sections from each case was processed according to an updated and simplified protocol for staining with aldehyde fuchsine (19) to visualize human lipofuscin pigment deposits (35) and then counterstained with Darrow red for visualization of basophilic material (19, 34, 36, 37) (see also Supplementary Data). A second and a third set of free-floating sections were processed with silver methods to visualize AD-related neurofibrillary changes (Gallyas silver-iodide) and Aβ plaques (Campbell-Switzer), as recommended elsewhere (34, 38, 39).

For immunohistochemistry, sets of free-floating sections were treated for 30 minutes in a mixture of 10% methanol plus 10% concentrated (30%) H_2O_2 and 80% Tris. Following pretreatment to facilitate the immunoreactions, blocking with bovine serum albumin was performed to inhibit endogenous peroxidase and to prevent nonspecific binding. Subsequently, each of the sets was incubated for 18 hours at 20°C using 1 of the following commercially available primary antibodies: (i) a monoclonal mouse antibody anti-β-amyloid (1:5000; 1 mg/mL; Clone 4G8; Covance, Dedham, MA) for detection of Aβ deposition (33); (ii) a monoclonal antibody against phosphorylated tau (PHF-Tau; 1:2000, 200 mg/mL; Clone AT8; Pierce Biotechnology, Rockford, IL) to detect AD-related pretangles, NFTs, and NTs (39), as well as lesions associated with other tauopathies. Sections immunostained for TDP-43 pathology were pretreated by steaming for 1 hour in citrate buffer before processing with (iii) a commercially available polyclonal rabbit antibody recognizing the N-terminal of all species of nuclear TDP-43 (non-phosphorylated, phosphorylated, monomeric, and polymeric) (1:2500, 46 µg/150 µL; Proteintech, Manchester, UK). Some of the AT8 and TDP-43 immunoreactions were combined with Darrow red counterstaining for topographical overview or with a combination of aldehyde fuchsine and Darrow red.

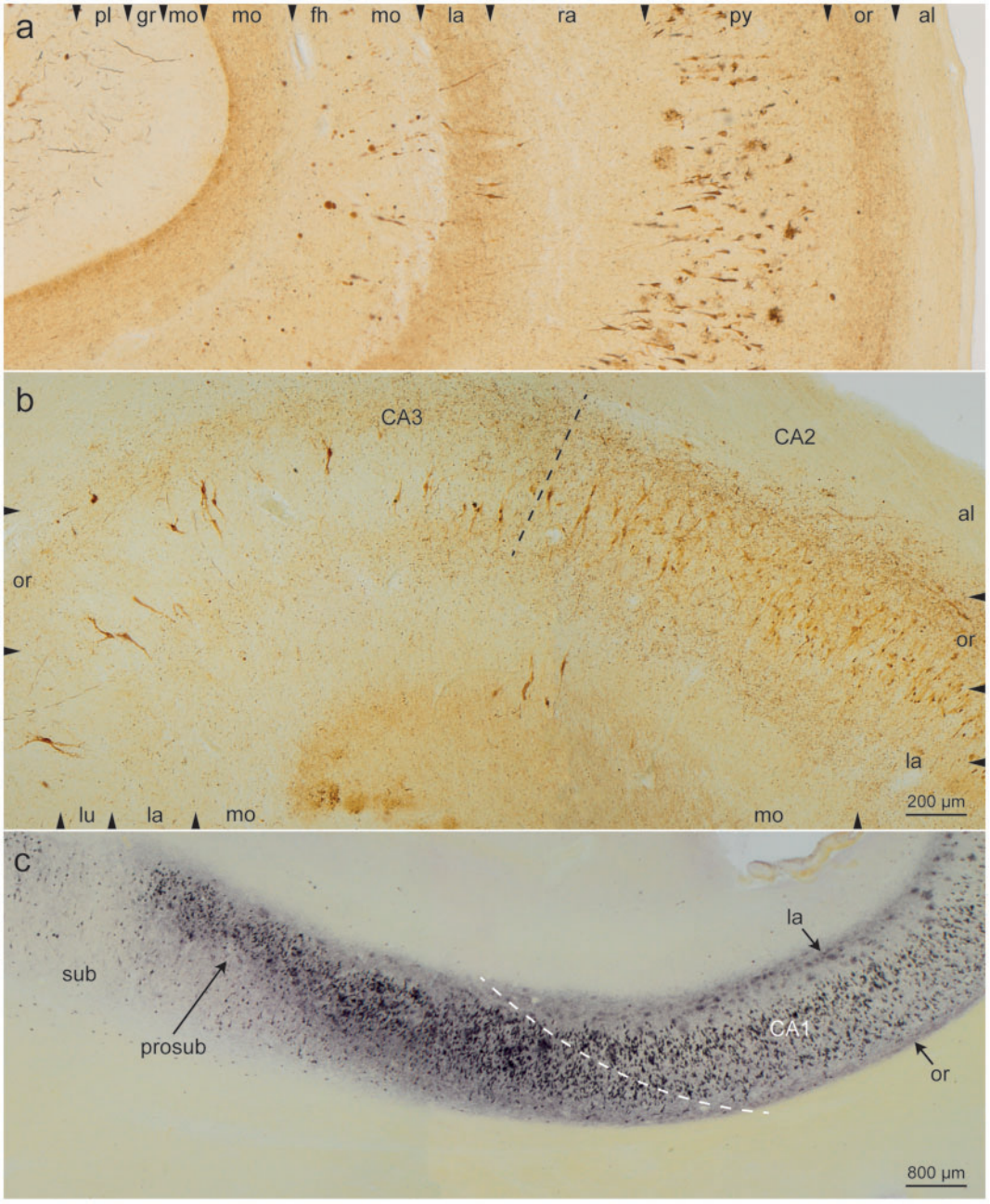

FIGURE 3. Detail micrographs from the same section as in Figure 2 (case 45, female, age 83, NFT III, Aβ 0). **(a)** In CA1, the pyramidal layer showed numerous AT8-positive somata. The myelin-rich alveus and stratum radiatum appeared as bright and almost immunonegative zones (al, ra). Similarly, the broad molecular layer between stratum lacunosum and the hippocampal fissure (fh, mo) was poor in AT8-positive structures with the exception of conspicuous enlargements of the terminal apical dendrites that frequently were accompanied by a tear in the layer (see asterisk in Fig. 2). In addition, the terminal zone of the perforant path in the middle and outer two-thirds of the dentate molecular layer displayed AT8-positive structures (mo). The granular layer and the inner third of the molecular layer of the dentate fascia were uninvolved and appeared as pallid zones (gr, mo). The micrograph, which corresponds to the framed area "a" in Figure 2, displays the 2 conspicuous stripes of accumulated NTs in the stratum oriens and stratum lacunosum of CA1. **(b)** This micrograph, which corresponds to the framed area "b" in Figure 2, shows the border between CA2 and CA3 (broken line). In CA2, the stripes in the stratum oriens and stratum lacunosum were still recognizable although less densely packed with NTs. Both stripes appeared again in sector CA3 but were less easily recognizable (see also Fig. 2). **(c)** Gallyas silver-iodide staining was used to show the beginning of the stripes in the prosubiculum and the gradual formation of argyrophilic NT accumulations in the stratum oriens (arrow or) and in the stratum lacunosum (arrow la). The subiculum was virtually spared of pathology (case 60, female, age 84, NFT IV, Aβ 2). Scale bars: **(b)** = 200 µm, also valid for **(a)**; **(c)** = 800 µm.

Subsequent to processing with a corresponding secondary biotinylated antibody (antimouse or antirabbit IgG, 1:200; Linaris, Vector Laboratories, Burlingame, CA) for 1.5 hours, all immunoreactions were visualized with the avidin-biotin complex (ABC, Vectastain, Vector Laboratories, Burlingame, CA) for 2 hours and the brown chromogen 3,3-diaminobenzidine tetrahydrochloride (DAB, D5637 Sigma, Taufkirchen, Germany) or the blue chromogen SK 4700 (SG Substrate Kit, Vector Laboratories). Omission of the primary antiserum resulted in nonstaining. Positive as well as negative control sections were included for all immunoreactions.

The tissue sections were cleared, mounted, and coverslipped (Histomount, National Diagnostics, Atlanta, GA). Slides were viewed and neuropathological staging performed with an Olympus BX61 microscope (Olympus Optical, Tokyo, Japan). Digital micrographs were taken with an Olympus XC50 camera. The extended focal imaging (EFI) function was used for stacks of images at different optical planes (Cell D Imaging Software, Olympus, Münster, Germany). The EFI algorithm extracts the image features with the sharpest contrast from all layers of the stack and merges them into a single image.

RESULTS

Development of Abnormal Distal Dendrites in the Transentorhinal and Entorhinal Regions Around Layer Pre-α Projection Cells

Cases with the mildest cortical affection (NFT stage I) showed a combination of AT8-positive dots and NTs in distal dendritic segments of projection neurons in layer pre-α of the transentorhinal and entorhinal regions (40, 41). Interneurons or nerve cells in other cortical layers did not display abnormal tau. Spines along the involved dendrites did not display AT8-positive accumulations. Subsequently, abnormal tau was seen within the cell somata and proximal portions of the axon of involved pre-α cells. Then, the distal dendritic segments of these cells displayed curved and thickened processes that could be followed only for short distances. Proximal dendrites, that is, the compartment between the distal dendritic segments and the cell body, were not AT8-positive.

The dendritic tips of pre-α cells did not form a continuous network or plexus but appeared as dense accumulations of single nerve cell processes accompanied by AT8-positive dots and twigs (16, 42). All of the abnormal cell compartments seen up to this point were Gallyas-negative (nonargyrophilic) and, thus, were identified as pretangles (14, 15). Involved cells then developed Gallyas-positive argyrophilic dendritic NTs and somatic NFTs. These extended widely into dendritic stems but not into the axon, where accumulations of abnormal tau remained nonargyrophilic.

Development of Abnormal Distal Dendrites in the Prosubiculum With Progression into the Stratum Oriens and Stratum Lacunosum of Sector CA1

AT8-immunoreactive distal dendrites (NTs) then occurred in the hippocampal formation (Figs. 2 and 3). Beginning in the prosubiculum, they formed 2 distinct stripe-like layers, 1 basal and 1 superficial (Figs. 2 and 3). The basal stripe corresponded to the stratum oriens of CA1 (Figs. 2 and 3a), and nerve cells within this stratum did not display abnormal tau changes. The superficial stripe extended into the stratum lacunosum (Figs. 2 and 3a) and also contained AT8-positive axons of the perforant path (Figs. 1 and 4f). Additional NTs were present loosely distributed between the stripe-like zones of the stratum oriens and stratum lacunosum (Figs. 2 and 3a). Furthermore, the terminal zone of the perforant path in the middle and outer two-thirds of the dentate molecular layer displayed AT8-positive axon-like structures (Figs. 2 and 3a) (43, 44).

After the development of distal NTs in the stratum oriens and stratum lacunosum of CA1, abnormal tau was seen in the somata of CA1 pyramids (Fig. 4a, c) (isolated cells at NFT stage I, several more in NFT stage II). Pretangles there (Fig. 4g, i) converted into filamentous argyrophilic NFTs (Fig. 4h). In addition, involved pyramidal cells displayed changes within their apical dendrites. This phenomenon occurred mostly in centrally located pyramidal cells located close to the edge of the lateral ventricle (Fig. 4b). The dense filling of the main dendrite with abnormal tau extended upwards to the terminal tuft close to the hippocampal fissure (Fig. 4b[hf]) and showed (beyond the NTs already present in the stratum lacunosum; Fig. 4b[la]) growing numbers of AT8-positive spindle-shaped enlargements in the molecular layer (Figs. 3a and 4b[mo]). The continuity between the portions with enlargements was maintained by thread-like segments of the apical dendrite. Many of the abnormally changed segments converted to argyrophilic structures (Fig. 4d) and were detached from the soma, leaving behind dendritic remnants as detritus (Fig. 4d). The remaining somata appeared unchanged (45), but the loss of portions of the dendritic arbor made the tissue increasingly brittle, as seen in torn portions along the hippocampal fissure.

Development of Abnormal Distal Dendrites in Sectors CA2/CA3 and of AT8-Positive Thorny Excrescences in Sectors CA3/CA4

The stripe-like (bilaminar) zones of NTs in both the stratum oriens and stratum lacunosum of sector CA1 extended into less densely packed but broader zones of the CA2 sector (Figs. 2 and 3b). In CA3, the stratum lacunosum-moleculare followed rather abruptly on the stratum lucidum (Figs. 2 and 3b). In addition, numerous NTs were scattered within the stratum pyramidale of sector CA2, so that in CA2 all 3 strata (oriens, pyramidale, and lacunosum) could be subsumed into a single zone filled with altered distal dendritic segments (Figs. 2 and 3b).

In CA2, pretangles developed in cell somata in a manner different from that seen in CA1: Abnormal tau accumulated very slowly and was evenly distributed throughout the cell soma (Fig. 5a, b). Rarely, a few compact and rounded AT8-positive inclusions were present in the cytoplasm (Fig. 5c, d). In addition, a thin film of abnormal tau consistently

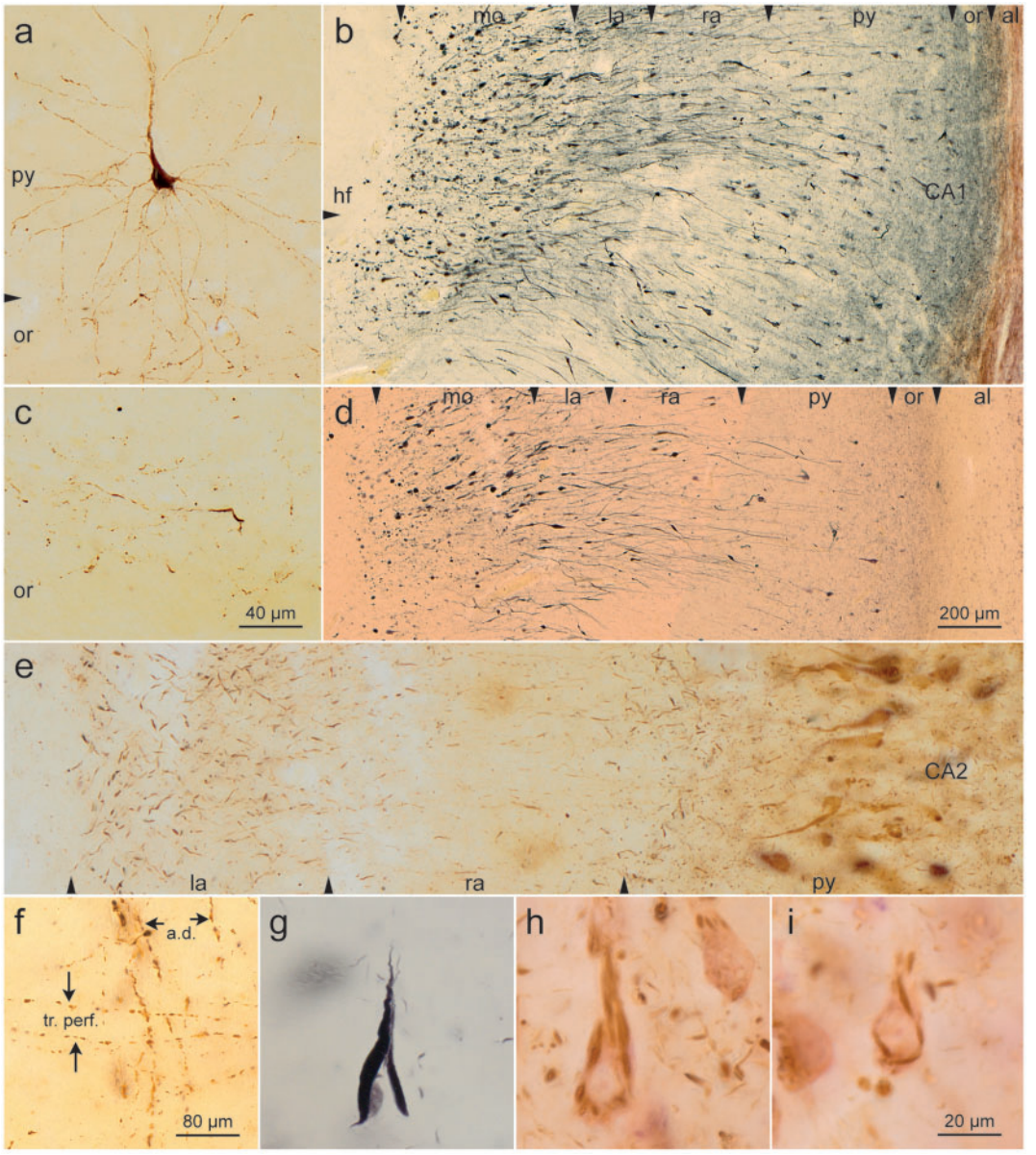

FIGURE 4. Somatic alterations of CA1 projection neurons. **(a**, **c)** Early development of abnormal tau in a CA1 pyramidal cell. Note changes in distal segments of the basal dendrites that reach into the stratum oriens. **(c)** A portion of the stratum oriens in an early phase of development (AT8, case 23, male, age 64, NFT II, Aβ 0). **(b**, **d)** CA1 pyramidal cells are prone to develop alterations of their apical dendrite. Their terminal portions in the molecular layer (mo) develop, extensions interconnected by thread-like segments (AT8, blue chromogen). The same case seen in Gallyas silver-iodide (case 7, male, age 69, NFT I, Aβ 0). In both micrographs, the lateral ventricle (not shown) would be located at the far right (see also Fig. 3a). **(e)** Apical dendrites of CA2 pyramidal cells show a less conspicuous but basically similar change with thickenings of their terminal segments (AT8, case 26, female, age 82, NFT II, Aβ 1). **(f)** Stratum lacunosum of CA1. Apical dendrites of CA1-pyramidal cells (a. d.) and involved axons of the perforant path (tr. perf.) (AT8, case 22, male, age 64, NFT II, Aβ 0). Altered CA1 cells. **(g)** Mature argyrophilic neurofibrillary tangle of a CA1 pyramidal cell (Gallyas silver-iodide staining). **(h**, **i)** Flake-like formation of fibrillized tangle in CA1 pyramidal cells. Note the absence of perinuclear pretangle material (AT8, case 60, female, age 84, NFT IV, Aβ 2). Scale bars: **(c)** = 40 µm, also applies to **(a)**; **(d)** = 200 µm, also applies to **(b)**; **(f)** = 80 µm; **(i)** = 20 µm, also applies to **(e)**, **(g)**, and **(h).**

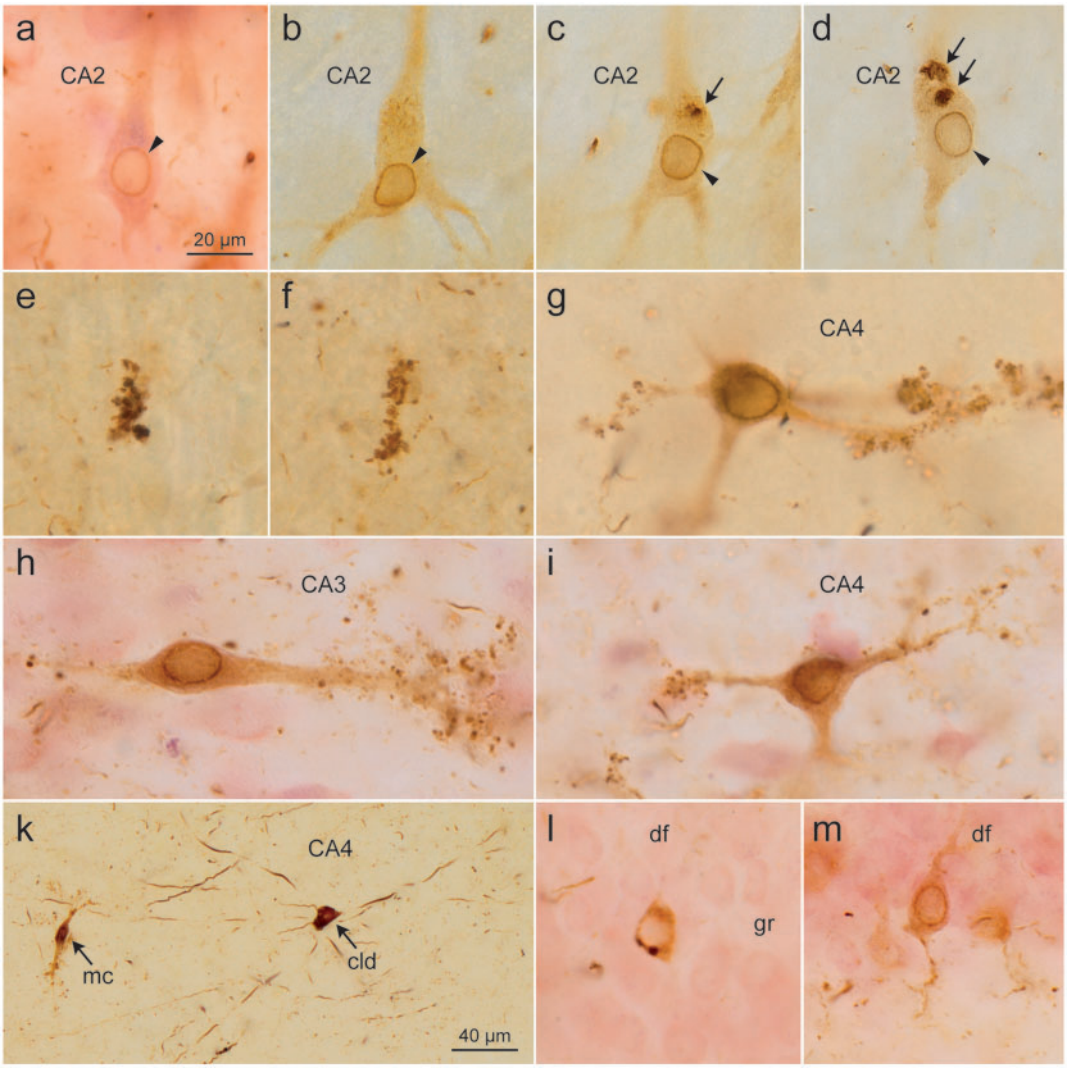

FIGURE 5. Pretangles in CA2 cells developed gradually and were evenly distributed throughout the somatodendritic compartment, consistently showing perinuclear tau accumulation (arrowheads). **(c, d)** A few rounded accumulations of densely packed abnormal tau (arrows) occasionally occurred in the cytoplasm [**(a)** case 60, female, age 84, NFT IV, Aβ 2; **(b–d)** case 75, male, age 80, NFT V, Aβ 2]. **(e, f)** The earliest changes in CA3/CA4 were small AT8-immunoreactive dots that occur in isolation and resemble dendritic excrescences (case 75, male, age 80, NFT V, Aβ 2). These cells showed characteristic excrescences along their dendrites and, similar to CA2 cells, exhibited a zone of perinuclear tau accumulation [**(g)** case 45, female, age 83, NFT III, Aβ 0; **(h, i)** case 60, female, age 84, NFT IV, Aβ 2]. **(k)** The first cells involved in CA4 usually belonged to the type of multipolar pigment-laden cells with long and smoothly contoured dendrites without excrescences (arrow: cld). For comparison, a typical CA4 mossy cell is shown at the left (arrow: mc) (case 45, female, age 83, NFT III, Aβ 0). The last cells to develop changes were the granule cells (gr) of the dentate fascia (df). These cells showed a uniformly distributed AT8-positive tau in the cytoplasm as well as perinuclear tau accumulations. **(l)** Rarely, AT8-positive dots were seen in the cytoplasm. **(m)** Distal dendritic segments did not show spindle-shaped enlargements (case 60, female, age 84, NFT IV, Aβ 2). Scale bars: **(a–i, l, m)** = 20 µm; **(k)** = 40 µm.

accumulated close to the cell nucleus (Fig. 5a–d). At the border between CA1 and CA2, pyramidal cells showing perinuclear AT8-immunoreactivity (as in CA2) were intermingled with pyramidal cells without perinuclear AT8-immunoreactivity (as in CA1).

Involved CA2 pyramids displayed changed apical dendrites that were similar to those seen in CA1 projection neurons (Fig. 4e). Once again, it was the terminal tuft of the apical dendrite within the stratum lacunosum-moleculare that contained slender spindle-shaped enlargements (Fig. 4e). However, there was no evidence that the altered apical dendrites were disconnected from the soma.

In NFT stage III or IV, abnormal tau also appeared in the pyramidal layer of CA3, at first as dot- or ring-like structures (i.e. thorny excrescences) that initially lay isolated in the neuropil (Fig. 5e, f) but subsequently were also seen along dendrites of CA3 mossy cells (Fig. 5h) (46). Then, as in CA2, abnormal tau spread throughout the somata of CA3 mossy

cells. As in CA2, the perinuclear zone was AT8-positive (Fig. 5h). Notably, this ring-like zone did not become argyrophilic. The spindle-shaped neurons in both the stratum oriens and stratum lacunosum of CA2-CA3 were free of AT8-immunoreactive tau.

In CA4, AT8-positive dendritic tips lay scattered amidst a few large AT8-positive projection cells that were lipofuscin-rich and had remarkably long, smoothly contoured dendrites (Fig. 5k[cld]). Notably, these cells displayed neither perinuclear abnormal tau nor thorny excrescences. In contrast to these, multipolar mossy cells, the predominate cell type of CA4, then developed tau lesions and exhibited the same abnormal features as the pyramidal mossy cells in CA3 (Fig. 5k[mc], g, i).

Development of Abnormal Tau in Granule Cells of the df

An increasing number of granule cells in the df became AT8-positive and then argyrophilic in NFT stages V and VI (Fig. 5l, m). The perinuclear zone of involved granule cells was AT8-positive (Fig. 5l, m). The terminal tips of granule cell dendrites were not enlarged in contrast to what was seen elsewhere in the hippocampal formation. Together with granule cell involvement, AT8-positive axon-like structures were found in the inner one-third of the dentate molecular layer.

DISCUSSION

The findings reported above rest on a cross-sectional study of 95 individuals at different NFT stages (Table). Cross-sectional studies necessitate a hypothetical timeline and have both advantages as well as shortcomings (47). Here, the proposed progression of tau lesions in the temporal allocortex was ordered according to the regional extent and increasing severity of the lesions. Such a sequence can only be posited when 1 assumes that the pathological process progresses in a uniform manner and leaves behind its footprints in the form of neuronal accumulations of abnormal tau (48, 49).

Initially, a single type of cortical projection cell in the transentorhinal and entorhinal regions was involved (pre-α cells) and gradually followed by a few additional cell types. It looks thereby as though the pathological process could undergo a transfer from a well-defined neuronal type to additional well-defined but still uninvolved nerve cells via axonal connectivities (48–53). Although it is not the only possible modus of transmission (54, 55), the mechanisms of seeding and transsynaptic transmission of abnormal tau from 1 nerve cell to the next cell in the neuronal chain is 1 of the simplest and most elegant explanations for the progression of tau pathology in the sAD brain (56–63).

It is important for the further analysis to realize that the unidirectional sequence of connections from dentate granule cells to subicular pyramidal cells (Fig. 1, short red arrows) is not compatible with the sequence of the abnormal tau lesions we proposed in "Results" ([20, 44, 64–72], see also Supplementary Data). Notably, the dentate granule cells and the mossy fiber system do not become involved in early NFT stages and, even in later NFT stages, the stratum lucidum remains spared or displays almost no tau pathology (3). Also uninvolved is the ensuing system of CA3 mossy cells and Schaffer collaterals. The stratum radiatum of CA1 stays nearly intact until NFT stages V–VI (Figs. 2 and 3a). Similarly, the projections of CA1 pyramidal cells to the apical dendrites of subicular pyramidal cells remain intact, and the large subicular pyramidal cells become only minimally involved in late NFT stages (Fig. 3c). In other words, the sAD-related pathological process does not use the known hippocampal unidirectional connections (Fig. 1, short red arrows). The sequence we propose runs in the opposite direction (Fig. 1, green arrows vs red arrows). However, direct connections between layer pre-α cells and the stratum oriens of CA1 (Fig. 1) as well as between CA1 or prosubiculum and excrescences of CA3 mossy cells have not been verified in anatomical studies (20, 73).

The problem with the directionality we propose recalls the discussion about "bottom-up" versus "top-down" progression of sAD-related neurofibrillary changes within the neocortex: Cortical cells that send projections via the small spiny stellate cells of neocortical layer IV to higher order association areas (bottom-up projections) do not become involved in sAD, not even in NFT stages V and VI (19). The alternatives, that is, the top-down pathways, project—via all cellular layers except layer IV—in the opposite direction and bear the brunt of the pathology. Our proposed sequence of tau lesions in the allocortex resembles the directionality seen in the neocortex, where the tau pathology appears to use chiefly the top-down connectivities (19). However, because similar connections in the hippocampal formation are unknown in humans or hominids, we can only speculate about their possible existence based on the abnormal tau lesions we saw there (Fig. 1, green arrows).

The earliest changes seen in the temporal allocortex during NFT stages I–II consisted of AT8-positive dots along axon-like structures and abnormal tau in distal dendritic segments (NTs) of projection neurons of layer pre-α (40, 74, 75). The AT8-positive dots could have been twigs or terminal axons belonging to subcortical nuclei that project to this cortical layer. These nuclei with diffuse cortical projections are the only nuclei known to become involved prior to layer pre-α and include the locus coeruleus, upper raphe nuclei, and the magnocellular nuclei of the basal forebrain (3, 76).

During this initial phase, the somata of involved pre-α neurons remained AT8-negative, which indicates that the abnormal tau in distal dendrites likely originated in dendrites rather than having been recruited from the axon and transported into the remote dendritic segments before undergoing a change of conformation and accumulation (19, 77–80). The abnormal distal dendrites (NTs) are hallmarks of the pathological tau process and have been used for neuropathological staging (10). Subsequently, they converted into argyrophilic NTs (14, 15) and partially surrounded pre-α cells, where they were seen between NFT stages I and VI. Notably, spiny appendages along affected dendrites remained AT8-immunonegative.

In NFT stages II and III, a similar combination of AT8-positive dots and abnormal distal dendrites as in pre-α occurred in the hippocampal formation, beginning with abnormal tau changes in the prosubiculum (Fig. 3c). The massed

distal dendrites were organized into a pronounced basal portion that filled the stratum oriens of CA1 and a superficial portion that extended into the stratum lacunosum (Figs. 2 and 3a, c).

The radially aligned NTs in the stratum oriens likely represented distal segments of basal dendrites of CA1 pyramidal cells. Nerve cells and their dendrites within the stratum oriens itself were tangentially aligned and remained unaffected. The pathology in the stratum oriens is not easy to explain. Part of the Schaffer collaterals terminate within this layer (Fig. 1) (20, 81); nevertheless, up to NFT stage III, the CA3 mossy cells were uninvolved and, thus, Schaffer collaterals could not be responsible for causing the development of abnormal distal dendrites in the stratum oriens during NFT stages I and II. Again, the existence of a direct connection from layer pre-α to the stratum oriens of CA1 (Fig. 1) has not been anatomically verified (20, 73).

The abnormal dendrites seen in the stratum lacunosum of CA1 were distal segments belonging to side-branches of the apical dendrites of CA1 pyramidal cells. The stratum lacunosum also contained AT8-positive axons of the perforant path that ran perpendicular to the apical dendrites (Fig. 4f). It is possible that dendrites in the stratum lacunosum received their tau pathology from seed-containing side-branches of the perforant path.

After the appearance of the first hippocampal lesions, abnormal tau developed in cell bodies of CA1 pyramidal cells (82). The small number of initially involved pyramidal cells there contrasted with the large number of abnormal dendrites in the 2 stripe-like zones in the stratum oriens and stratum lacunosum. Thus, we think that abnormal tau was temporarily confined to the dendritic tips of CA1 pyramidal cells. These circumscribed lesions did not result in cell death but could selectively damage phylo- and ontogenetically late-emerging synapses along the distal dendritic segments (83, 84). In the neocortex, for instance, proximal portions of pyramidal cell dendrites function as contact zones for phylogenetically early-appearing bottom-up projections that reach these proximal dendrites via layer IV spiny stellate cells, that is, they follow the same direction as the unidirectional connections of the allocortex (Fig. 1). We assume that, at the end of this developmental phase, not only in the neocortex but also in the allocortex the pyramidal cell dendrites of humans and higher primates continue to sprout and to produce new distal twigs, which then would provide additional sites for new synapses of axons. In the neocortex, these new connections are provided by the top-down projections. In the allocortex, they represent the here hypothesized projections that run in the opposite direction to known allocortical unidirectional connectivities.

The number of involved cell bodies in CA1 increased, and filamentous argyrophilic NFTs appeared. In addition, involved CA1 pyramids displayed severe alterations in terminal twigs of their apical dendrite that eventually became disconnected from the soma (Fig. 4b, d). Such "amputated" neurons would undergo a loss of function. Because altered apical dendrites were seen only after the appearance of abnormal dendrites in the stratum lacunosum, it is possible that these early changes caused the abnormalities of the apical dendrite. Additional studies are needed to see if this is true and, if so, how, in detail, these changes come about.

After the pathological changes in CA1, abnormal tau developed in CA2-CA4 in NFT stages III or IV. The stripe-like accumulations of abnormal dendritic tips in the stratum oriens and stratum lacunosum of CA1 progressed further into the stratum oriens and stratum lacunosum of CA2-CA3 as more loosely organized stripes (Figs. 2 and 3b). Abnormal tau also began to develop in isolated thorny excrescences of CA3/CA4 mossy cells (Fig. 5e, f). This is an unusual and unexpected finding: Normally, spines along dendrites of cortical projection cells remain negative in AT8-immunoreactions. Up to this point, the pathological process had not reached dentate granule cells; therefore, involved mossy fibers cannot have been the source of the immunoreactive material in thorny excrescences in CA3/CA4.

In contrast to CA1, the abnormal tau in CA2-CA4 developed more gradually and was more evenly distributed throughout the somatodendritic compartment. In addition, a line-like accumulation of abnormal tau close to the cell nucleus (Fig. 5a–d, g–i) helped to distinguish CA2-CA4 projection cells from those in CA1. Taken together, these features differed from those in CA1 and suggest a mode of transmission via a further hypothetical connection that may begin in pyramidal cells of the prosubiculum or CA1, and synapse on dendritic tips of CA2-CA4 projection cells but also synapse directly on thorny excrescences of CA3/CA4 mossy cells (Fig. 1).

Once tau pathology was present in all aforementioned sectors of the Ammon's horn, the dentate granule cells developed AT8-positive and then argyrophilic NFTs during NFT stages V–VI. Here, again, a pathway is conceivable that runs in the opposite direction to that of the main connections (Fig. 1), with a possible point of departure in multipolar mossy cells of CA4, which send profuse axonal collaterals to the internal one-third of the dentate molecular layer (20, 85, 86). Alternative cells of origin for this connection could be the lipofuscin pigment-laden nerve cells that are the first cells to become involved in CA4.

In summary, the results and hypotheses from the present study require confirmation by independent investigations. Only then can we learn whether the changes in tau pathology within components of the temporal allocortex in sAD are attributable to some kind of selective vulnerability or whether heretofore unknown connectivities exist, which would make possible the sequence of abnormal tau progression that we observed.

ACKNOWLEDGMENTS

The authors are grateful to the patients and their families, who made brain donation possible. They also thank Ms Simone Feldengut (immunohistochemistry) and Mr David Ewert (graphics) from the University of Ulm.

REFERENCES

1. Hyman BT, van Hoesen GW, Hippocampal and entorhinal cortex cellular pathology in Alzheimer's disease. In: Chan-Palay V, Köhler C, eds, *The Hippocampus: New Vistas*. New York: Liss 1989:499–512

2. Duyckaerts C, Delatour B, Potier MC. Classification and basic pathology of Alzheimer disease. Acta Neuropathol 2009;118:5–36
3. Braak H, Del Tredici K. Neuroanatomy and pathology of sporadic Alzheimer's disease. Adv Anat Embryol Cell Biol 2015;215:1–162
4. Calderon-Garciduenas AL, Duyckaerts C. Alzheimer disease. Handb Clin Neurol 2017;145:325–37
5. Rademakers R, Crut M, Van Broeckhoven D. Genetics of early-onset Alzheimer dementia. ScientificWorldJournal 2003;3:497–519
6. Bertram L, Lill CM, Tanzi RE. The genetics of Alzheimer disease: Back to the future. Neuron 2010;68:270–81
7. Bertram L, Tanzi RE. The genetics of Alzheimer's disease. Prog Mol Biol Transl Sci 2012;107:79–100
8. Arendt T. Alzheimer's disease as a loss of differentiation control in a subset of neurons that retain immature features in the adult brain. Neurobiol Aging 2000;21:783–96
9. Braak H, Alafuzoff I, Arzberger T, et al. Staging of Alzheimer's disease-associated neurofibrillary pathology using paraffin sections and immunohistochemistry. Acta Neuropathol 2006;112:389–404
10. Alafuzoff I, Arzberger T, Al-Sarraj S. Staging of neurofibrillary pathology in Alzheimer's disease: A study of the BrainNet Europe Consortium. Brain Pathol 2008;18:484–96
11. Braak H, Thal DR, Ghebremedhin E, Del Tredici K. Stages of the pathologic process in Alzheimer disease: Age categories from 1 to 100 years. J Neuropathol Exp Neurol 2011;70:960–9
12. Duyckaerts C, Braak H, Brion J-P. PART is part of Alzheimer disease. Acta Neuropathol 2015;129:749–56
13. Mercken M, Vandermeeren M, Lübke U. Monoclonal antibodies with selective specificity for Alzheimer tau are directed against phosphatase-sensitive epitopes. Acta Neuropathol 1992;84:265–72
14. Bancher C, Brunner C, Lassmann H, et al. Accumulation of abnormally phosphorylated tau precedes the formation of neurofibrillary tangles in Alzheimer's disease. Brain Res 1989;477:90–9
15. Braak E, Braak H, Mandelkow EM. A sequence of cytoskeleton changes related to the formation of neurofibrillary tangles and neuropil threads. Acta Neuropathol 1994;87:554–67
16. Braak H, Braak E, Grundke-Iqbal I, Iqbal K. Occurrence of neuropil threads in the senile human brain and in Alzheimer's disease: A third location of paired helical filaments outside of neurofibrillary tangles and neuritic plaques. Neurosci Lett 1986;65:351–5
17. Ashford JW, Soultanian NS, Zhang SX, Geddes JW. Neuropil threads are collinear with MAP2 immunostaining in neuronal dendrites of Alzheimer brain. J Neuropathol Exp Neurol 1998;57:972–8
18. Uchihara T, Nakamura A, Yamazaki M, Mori O. Evolution from pretangle neurons to neurofibrillary tangles monitored by thiazin red combined with Gallyas method and double immunofluorescence. Acta Neuropathol 2001;101:535–9
19. Braak H, Del Tredici K. Spreading of tau pathology in sporadic Alzheimer's disease along cortico-cortical top-down connections. Cereb Cortex 2018;28:3372–84
20. Insausti R, Amaral DG. Hippocampal formation. In: Mai JK, Paxinos G, eds. *The Human Nervous System*, 3rd edn. San Diego: Academic Press 2012:896–942
21. Thal DR, Rüb U, Orantes M, Braak H. Phases of Aβ-deposition in the human brain and its relevance for the development of AD. Neurology 2002;58:1791–800
22. Braak H, Braak E. Argyrophilic grain disease: Frequency of occurrence in different age categories and neuropathological diagnostic criteria. J Neural Transm 1998;105:801–19
23. Malnar M, Hecimovic S, Mattsson N, et al. Bidirectional links between Alzheimer's disease and Niemann-Pick type C disease. Neurobiol Dis 2014;72:37–47
24. Dickson DW. Neuropathology of non-Alzheimer degenerative disorders. Int J Clin Exp Pathol 2009;3:1–23
25. Nag S, Yu L, Capuano AW, et al. Hippocampal sclerosis and TDP-43 pathology in aging and Alzheimer disease. Ann Neurol 2015;77:942–52
26. Ihara R, Vincent BD, Baxter MD, et al. Relative neuron loss in hippocampal sclerosis of aging and Alzheimer's disease. Ann Neurol 2018;84:741–53
27. Wilson RS, Yang J, Yu L, et al. Postmortem neurodegenerative markers and trajectories of decline in cognitive systems. Neurology 2019;92:e831–e840
28. Corder E, Saunders A, Strittmatter W, et al. Gene dose of apolipoprotein E and type 4 allelle and the risk of Alzheimer's disease in late-onset families. Science 1993;261:921–3
29. Poirier J, Davignon J, Bouthillier D, et al. Apolipoprotein E polymorphism and Alzheimer's disease. Lancet 1993;342:697–9
30. Ward A, Crean S, Mercaldi CJ, et al. Prevalence of apolipoprotein E4 genotype and homozygotes (APOE e4/4) among patients diagnosed with Alzheimer's disease: A systematic review and metaanalysis. Neuroepidemiology 2012;38:1–17
31. Wenneberg AM, Tosakulwong N, Lesnick TG, et al. Association of apolipoprotein E ε4 with transactive response DNA-binding protein 43. JAMA Neurol 2018;75:1347–54
32. Ghebremedhin E, Braak H, Braak E, Sahm J. Improved method facilitates reliable APOE genotyping of genomic DNA extracted from formaldehyde-fixed pathology specimens. J Neurosci Meth 1998;79:229–31
33. Klosen P, Maessen X, van den Bosch de Aguilar P. PEG embedding for immunocytochemistry: Application to the analysis of immunoreactivity loss during histological processing. J Histochem Cytochem 1993;41:455–63
34. Braak H, Braak E. Demonstration of amyloid deposits and neurofibrillary changes in whole brain sections. Brain Pathol 1991;1:213–6
35. Double KL, Dedov VN, Fedorow H, et al. The comparative biology of neuromelanin and lipofuscin in the human brain. Cell Mol Life Sci 2008;11:1669–82
36. Braak H. Architectonics of the Human Telencephalic Cortex. Berlin: Springer 1980:1–147
37. Braak H. Architectonics as seen by lipofuscin stains. In: Jones EG, Peters A, eds. Cerebral Cortex. Cellular Components of the Cerebral Cortex, Vol I. New York: Plenum Press 1984:59–104
38. Gallyas F. Silver staining of Alzheimer's neurofibrillary changes by means of physical development. Acta Morph Acad Sci Hung 1971;19:1–8
39. Hyman BT, Phelps CH, Beach TG, et al. National Institute on Aging-Alzheimer's Association guidelines for the neuropathologic assessment of Alzheimer's disease. Alzheimers Dement 2012;8:1–13
40. Braak H, Braak E. On areas of transition between entorhinal allocortex and temporal isocortex in the human brain. Normal morphology and lamina-specific pathology in Alzheimer's disease. Acta Neuropathol 1985;68:325–32
41. Taylor KI, Probst A. Anatomic localization of the transentorhinal region of the perirhinal cortex. Neurobiol Aging 2008;29:1591–6
42. Wharton SB, Minett T, Drew D, et al. Epidemiological pathology of tau in the ageing brain: Application of staging for neuropil threads (BrainNet Europe protocol) to the MRC cognitive function and ageing brain study. Acta Neuropathol Comm 2016;4:11–20
43. Hyman BT, Kromer LJ, van Hoesen GW. A direct demonstration of the perforant pathway terminal zone in Alzheimer's disease using the monoclonal antibody Alz-50. Brain Res 1988;450:392–7
44. Hyman BT, Hoesen GWV, Damasio AR. Memory-related systems in Alzheimer's disease: An anatomic study. Neurology 1990;40:1721–30
45. Braak E, Braak H. Alzheimer's disease: Transiently developing dendritic changes in pyramidal cells of sector CA1 of the Ammon's horn. Acta Neuropathol 1997;93:323–5
46. Blazquez-Llorca L, Garcia-Marin V, Merino-Serrais P, et al. Abnormal tau phosphorylation in the thorny excrescences of CA3 hippocampal neurons in patients with Alzheimer's disease. J Alzheimer Dis 2011;23:1–16
47. Dickson DW. The value of cross-sectional neuroanatomical studies as a conceptual framework for prospective clinicopathological studies. Neurobiol Aging 1997;18:382–6
48. Duyckaerts C, Uchihara T, Seilhean D, et al. Dissociation of Alzheimer type pathology in a disconnected piece of cortex. Acta Neuropathol 1997;93:501–7
49. Duyckaerts C, Seilhean D, Sazdovitch V, et al. Seeding and propagation of lesions in neurodegenerative diseases: A new paradigm. Bull Acad Natl Med 2015;199:809–19
50. de Calignon A, Polydoro M, Suárez-Calvet M, et al. Propagation of tau pathology in a model of early Alzheimer's disease. Neuron 2012;73:685–97
51. Liu L, Drouet V, Wu JW, et al. Trans-synaptic spread of tau pathology in vivo. PLoS One 2012;7:e31302

52. Furman JL, Vaquer-Alicea J, White CL, et al. Widespread tau seeding activity at early Braak stages. Acta Neuropathol 2017;133:91–100
53. Valero M, Menendez de la Prida L. The hippocampus in depth: A sublayer-specific perspective of entorhinal-hippocampal function. Curr Opin Neurobiol 2018;52:107–14
54. Lewis J, Dickson DW. Propagation of tau pathology: Hypotheses, discoveries, and yet unresolved questions from experimental and human brain studies. Acta Neuropathol 2016;131:27–48
55. Mudher A, Colin M, Dujardin S, et al. What is the evidence that tau pathology spreads through prion-like propagation? Acta Neuropathol Commun 2017;5:99–119
56. Saper CB, Wainer BH, German DC. Axonal and transneuronal transport in the transmission of neurological disease: Potential role in system degenerations, including Alzheimer's disease. Neuroscience 1987;23: 389–98
57. Su JH, Deng G, Cotman CW. Transneuronal degeneration in the spread of Alzheimer's disease pathology: Immunohistochemical evidence for the transmission of tau hyperphosphorylation. Neurobiol Dis 1997;4: 365–75
58. Goedert M, Clavaguera F, Tolnay M. The propagation of prion-like protein inclusions in neurodegenerative diseases. Trends Neurosci 2010;33: 317–25
59. Goedert M, Falcon B, Clavaguera F, Tolnay M. Prion-like mechanisms in the pathogenesis of tauopathies and synucleinopathies. Curr Neurol Neurosci Rep 2014 14;14:495
60. Lee S-J, Desplats P, Sigurdson C, et al. Cell-to-cell transmission of non-prion protein aggregates. Nat Rev Neurol 2010;6:702–6
61. Spillantini MG, Goedert M. Tau pathology and neurodegeneration. Lancet Neurol 2013;12:609–22
62. Ahmed Z, Cooper J, Murray TK, et al. A novel in vivo model of tau propagation with rapid and progressive neurofibrillary tangle pathology: The pattern of spread is determined by connectivity, not proximity. Acta Neuropathol 2014;127:667–83
63. Kaufman SK, Del Tredici K, Thomas TL, et al. Tau seeding activity begins in the transentorhinal/entorhinal regions and anticipates phosphor-tau pathology in Alzheimer's disease and PART. Acta Neuropathol 2018;136:57–67
64. Van Hoesen GW, Pandya DN. Some connections of the entorhinal (area 28) and perirhinal (area 35) cortices of the rhesus monkey. III. Efferent connections. Brain Res 1975;95:39–59
65. Van Hoesen GW, Hyman BT. Hippocampal formation: Anatomy and the patterns of pathology in Alzheimer's disease. Prog Brain Res 1990;83:445–57
66. Witter MP, Amaral DG. Entorhinal cortex of the monkey: V. Projections to the dentate gyrus, hippocampus, and subicular complex. J Comp Neurol 1991;307:437–59
67. Witter MP. Organization of the hippocampal-entorhinal system: A review of current anatomical data. Hippocampus 1993;3:33–44
68. Witter MP. The perforant path: Projections from the entorhinal cortex to the dentate gyrus. Prog Brain Res 2007;163:43–61
69. Gloor P. The Temporal Lobe and Limbic System. New York: Oxford University Press 1997:1–865
70. Andersen P, Morris R, Amaral D, et al. The Hippocampus Book. New York: Oxford University Press 2006
71. Böhm C, Peng Y, Geiger JRP, Schmitz D. Routes to, from and within the subiculum. Cell Tissue Res 2018;373:557–63
72. Christensen KR, Beach TG, Serrano GE, Kanaa NM. Pathogenic tau modifications occur in axons before the somatodendritic compartment in mossy fiber and Schaffer collateral pathways. Acta Neuropathol Comm 2019;7:29–50
73. Rosene DL, van Hoesen G. The hippocampal formation of the primate brain. In: Jones EG, Peters A, eds. Cerebral Cortex. Vol 6. New York: Plenum Press 1987: 345–56
74. Braak H, Braak E. The human entorhinal cortex: Normal morphology and lamina-specific pathology in various diseases. Neurosci Res 1992; 15:6–31
75. Insausti R, Muñoz-López M, Insausti AM, Artacho-Pérula E. The human periallocortex: Layer pattern in presubiculum, parasubiculum and entorhinal cortex. A review. Front Neuroanat 2017;11:84
76. German DC, White CL, Sparkman DR. Alzheimer's disease: Neurofibrillary tangles in nuclei that project to the cerebral cortex. Neurosci 1987; 21:305–12
77. Tashiro K, Hasegawa M, Ihara Y, Iwatsubo T. Somatodendritic localization of phosphorylated tau in neonatal and adult rat cerebral cortex. Neuroreport 1997;8:2797–801
78. Ittner LM, Ke YD, Delerue F, et al. Dendritic function of tau mediates amyloid-beta toxicity in Alzheimer's disease mouse models. Cell 2010; 142:387–97
79. Tai HC, Serrano-Pozo A, Hashimoto T, et al. The synaptic accumulation of hyperphosphorylated tau oligomers in Alzheimer disease is associated with dysfunction of the ubiquitin-proteasome system. Am J Pathol 2012; 181:1426– 5
80. Merino-Serrais P, Benavides-Piccione R, Blazquez-Llorca L, et al. The influence of phospho-tau on dendritic spines of cortical pyramidal neurons in patients with Alzheimer's disease. Brain 2013;136: 1913–28
81. Lim C, Mufson EJ, Kordower JH, et al. Connections of the hippocampal formation in humans. II. The endfolial fiber pathway. J Comp Neurol 1997;385:352–71
82. Benavides-Piccione R, Regalando-Reyes M, Fernaud-Espinosa I, et al. Differential structure of hippocampal CA1 pyramidal neurons in the human and mouse. Cereb Cortex 2019; doi:10.1093/cercor/bhz122 [Epub ahead of print]
83. Häusser M, Mel B. Dendrites: Bug or feature? Curr Opin Neurobiol 2003;13:372–83
84. Branco T, Häusser M. Synaptic integration gradients in single cortical pyramidal cell dendrites. Neuron 2011;69:885–92
85. Lim C, Blume HW, Madsen JR, Saper CB. Connections of the hippocampal formation in humans. I. The mossy fiber pathway. J Comp Neurol 1997;385:325–51
86. Scharfman HE. Advances in understanding hilar mossy cells of the dentate gyrus. Cell Tissue Res 2018;373:643–52